Theoretical and numerical comparison of different poloidal correlation reflectometry schemes

O.L. Krutkin[1,2], E.Z. Gusakov[1], P. Aleynikov[3], A.B. Altukhov[1], A.D. Gurchenko[1], L.A. Esipov[1], T.P. Kiviniemi[4], S. Leerink[4], P. Niskala[4]

[1]*Ioffe Institute, St Petersburg, Russia*
[2]*École polytechnique fédérale de Lausanne, Lausanne, Switzerland*
[3]*Max-Planck-Institut für Plasmaphysik, Greifswald, Germany*
[4]*Aalto University, Espoo, Finland*

Introduction

One of the major goals of magnetically confined fusion research is the understanding and control of plasma turbulence, which deteriorates the confinement of plasma. The tools used to study turbulence experimentally include microwave diagnostics and, in particular, poloidal correlation reflectometry (PCR) [1][2][3].

The PCR diagnostic is used to measure the poloidal rotation velocity of the plasma as well as turbulence poloidal correlation length and decorrelation time. It utilizes plasma probing (normally to the magnetic surface) in the presence of the cut-off. As the probing microwaves are scattered by turbulent density perturbations, the scattering signal is measured by two receiver antennas shifted in poloidal direction. The cross-correlation function (CCF) of the two signals is assumed to correspond to the two-point CCF of the density perturbations between the two turning points corresponding to the probing waves.

The standard experimental setup (Fig. 1a) involves receivers shifted poloidally in opposite directions. At the first glance such a configuration, possessing inversion symmetry, would provide information on the fluctuations with the opposite sign of poloidal wavenumber, but in the case of statistically homogeneous turbulence they would not correlate with each other. Therefore, one would expect a configuration possessing translational symmetry (Fig. 1b) to be superior. This conclusion was in fact achieved within the study of nonlinear scattering regime of PCR [4].

Thus, the goal of this work was the linear theoretical analysis of the PCR diagnostic as well as validation of the results with numerical modelling. In particular, it involved the comparison of the two aforementioned configurations.

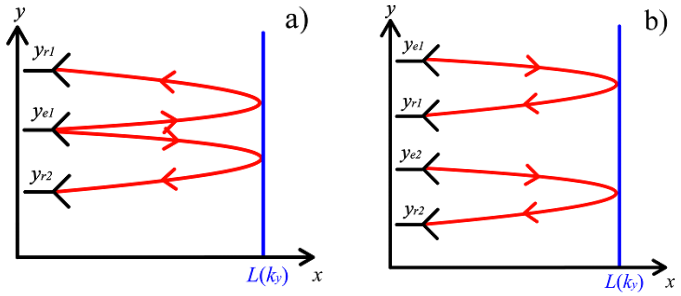

Fig. 1. Illustration of the different probing configurations. The vertical line at $x=L(k_y)$ designates the turning point.

Theoretical analysis

In this work, the perturbation theory approach is applied to the Helmholtz equation. Slab geometry of the model presented on the Fig. 1. In case of O-mode probing, Helmholtz equation takes the form:

$$\frac{\partial^2}{\partial x^2}E(x,y)+\frac{\partial^2}{\partial y^2}E(x,y)+\frac{\omega^2}{c^2}\left(1-\frac{n(x,y)}{n_c}\right)E(x,y)=0; \quad (1)$$

Here, ω stands for the probing frequency, $n(x,y)$ is the electron density and $n_c=m_e\omega^2/4\pi e^2$ is the critical density corresponding to the O-mode cut-off. We separate the density profile into

background density, uniform along the poloidal direction, and density perturbation: $n(x,y)=n_0(x)+\delta n(x,y)$. A linear background density profile $n_0(x) = n_c\, x/L$ is assumed, which means the solution E^0 to the unperturbed equation (1) is given by the Airy function.
Repeating the principles of derivation in [5][6], we will rely on the reciprocity theorem [7] to obtain the linear scattering signal:

$$A_s = \frac{ie^2\sqrt{P}}{4m_e\omega}\int_0^{\infty}\int_{-\infty}^{\infty}\frac{\delta n(x,y)}{n_c}E^0(x,y)^e E^0(x,y)^r\,dxdy; \tag{2}$$

Assuming a Gaussian antenna pattern (with beam waist ρ), one arrives to the following:

$$A_s = -\frac{i^{1/2}e^2\sqrt{P}}{m_e c^2}\frac{\alpha^2\rho}{\sqrt{\pi}}\int_{-\infty}^{\infty}\int_{-\infty}^{\infty}\frac{\delta n(\kappa,q)}{\sqrt{\kappa\alpha}n_c}\left[\frac{1}{2}\frac{d^2\Phi}{dk_y^2}\right]^{-1/2}\exp\left[i\frac{\kappa^3\alpha^3}{12}+i\left(\left(\frac{q}{2}\right)^2\alpha^2-L/\alpha\right)\kappa\alpha\right] \tag{3}$$

$$\times\exp\left[-i\frac{4}{3}\left(\frac{L(-q/2)}{\alpha}\right)^{3/2}-\left(\frac{q}{2}\right)^2\rho^2+i\left(y_e+y_r\right)q/2-i\frac{1}{4}\frac{\left(y_r-y_e\right)^2}{\kappa\alpha^3-q^2\alpha^3/\kappa+2Lc/\omega+i\rho^2}\right]d\kappa dq$$

Here q and κ represent poloidal and radial wavenumbers of the turbulence, while y_e and y_r are poloidal positions of emitter and receiver antennas, and α is the Airy scale.
From this formula it can already be concluded that there is no dependence on the sign of y_r-y_e, meaning that there is no selection of turbulence with opposite signs of poloidal wavenumber for the three antenna configuration. The only term in (3) that depends on probing direction is the last exponential term, but it is proportional to $(y_r$-$y_e)^2$, ignoring the sign of antenna shift.
This result suggests that there is no principal difference between the two configurations. A qualitative illustration of this fact is given in Fig. 2. As it can be seen from the picture, for both receiving antennae, the scattering signal corresponding to the specific wavenumber q will be received. Moreover, the same poloidal harmonics will participate in the scattering, leading to the same amplitude of the received signal when combined with antenna pattern. In this case, the attenuation of the harmonic marked "***ray 2***" in the emitter will be reproduced by attenuation of the scattered wave "***ray 1****" by the receiver. Thus, even though the scattering off positive q is somewhat unexpected for the pair e1-r1, it still happens just as effectively as for e1-r2.

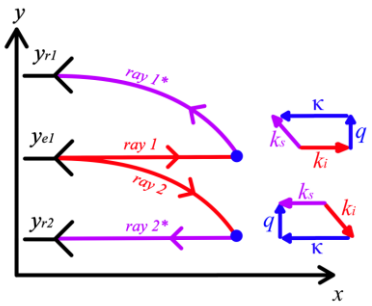

Fig. 2. Illustration of the scattering off the same turbulence for different antenna positions. k_i and k_s correspond to wave vector of the probing and scattered waves

Using formula (3), the expression for the CCF can be obtained for the Gaussian turbulence spectrum:

$$CCF(\tau) = 8\frac{\pi^2e^4P}{m_e^2c^4}\alpha^3 l_{cy}l_{cx}\frac{\delta n^2}{n_c^2}\mathrm{e}^{-\frac{\tau^2}{t_c^2}}\int_{-\infty}^{\infty}\int_{-\infty}^{\infty}\frac{\exp\left[i(\Delta\bar{y}-V\tau)q-\left(\kappa^2l_{cx}^2+q^2\left(l_{cy}^2+2\rho^2\right)\right)/4\right]}{\sqrt{\left(q^2\alpha^3-\kappa 2Lc/\omega\right)^2/\rho^4+\kappa^2}} \tag{4}$$

$$\times\exp\left[-\frac{1}{2}\frac{\rho^2\Delta y^2}{\left(2Lc/\omega-q^2\alpha^3/\kappa\right)^2+\rho^4}\right]d\kappa dq;\quad \Delta\bar{y}=\left(y_{e1}+y_{r1}-y_{e2}-y_{r2}\right)/2;\Delta y=y_r-y_e.$$

Here, l_{cx} and l_{cy} correspond to fluctuation correlation lengths and V is its poloidal velocity.
Formula (4) can be further simplified in the case of Δy=0, resulting in the expression:

$$CCF(\tau) \propto \exp\left[-\frac{(\Delta\bar{y}-V\tau)^2}{l_{cy}^2+2\rho^2}\Theta-\frac{\tau^2}{t_c^2}\right] \quad (5)$$

Here Θ is a factor with a value 0.7-0.9 for relevant parameters. This formula, aside from the factor Θ, goes in line with the traditional interpretation of the PCR measurements [8].

Numerical verification

To confirm analytically obtained conclusions, numerical modelling was performed. The data used for the task was a realistic turbulence produced with gyrokinetic full-f global ELMFIRE code [9] for the FT-2 tokamak. The ELMFIRE results were previously extensively benchmarked both directly [10] and indirectly [11] against experimental measurements and are expected to give a realistic turbulence data for the computation of the PCR CCF. The parameters of the ohmic discharge used for ELMFIRE modelling as well as the computation details can be found in [10], [11].

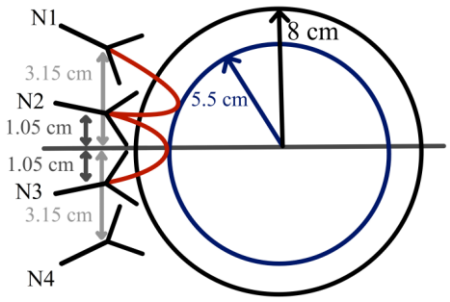

Fig. 3. Antenna setup used for numerical modelling

To obtain the PCR signals, the main approach used in this paper is the fast synthetic diagnostics of the ELMFIRE data within the linear approximation [12]. The method consists of computing the unperturbed field E^0 and integrating it with the density perturbations as prescribed by the reciprocity theorem (formula (3)). E^0 was computed using full-wave modelling with the full-wave code CUWA [13]. The field then was integrated with the density fluctuations provided by ELMFIRE. The geometry of the CUWA computation is given in Fig. 3.

The resulting synthetic CCF, cross-phase and spectra are presented on fig. 3-5 respectively:

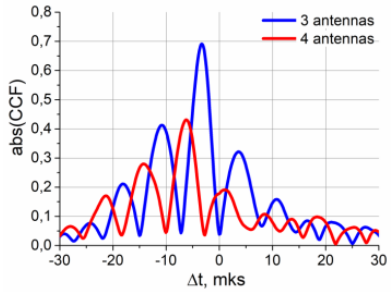

Fig. 4. The PCR *CCF*. Blue and red – two antenna configurations.

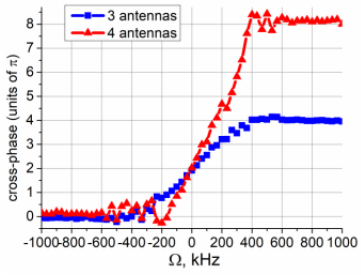

Fig. 5. Cross-phase. Blue and red – two antenna configurations.

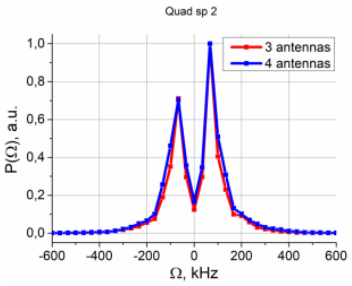

Fig.6. Power spectra. Blue and red – two antenna configurations.

In agreement with formula (5), both configurations produce qualitatively similar results. Larger value of $\bar{y}$ for the 4 antenna case ($\bar{y}_4 \approx 2\,\bar{y}_3$) results in a larger shift of the CCF maximum and its lower value. Accordingly, cross-phase changes roughly twice as fast in case of four antenna configuration. Finally, the coincidence of the spectra for the two configurations also is in agreement with formula (5).

Next, we performed a number of computations to test out the limits of obtained theoretical results. The computations were performed for X-mode probing, as it is used in actual FT-2 experiment.

The first limiting factor of the model is the use of slab geometry, which was implemented in computation by aligning antennas radially (Fig. 3). The result of a computation with horizontally aligned antennas is presented on Fig. 7. While the results for O-mode are not

shown in this work, they also demonstrate strong decay of correlation, which leads us to a conclusion that antenna misalignment can be a serious issue in experiment.

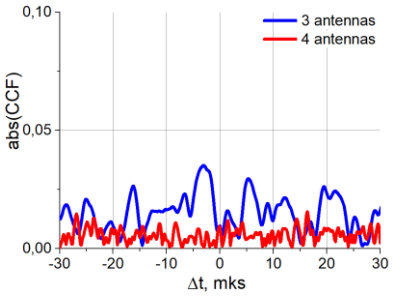

Fig.7. The PCR *CCF* for horizontal probing.

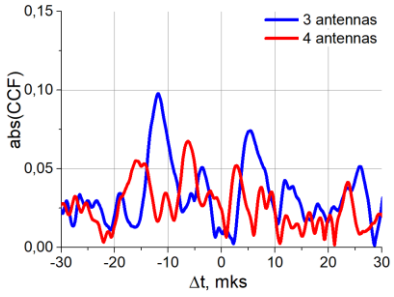

Fig. 8. The PCR *CCF* for raw ELMFIRE data.

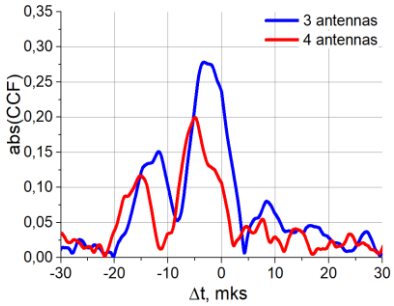

Fig.9. The PCR *CCF* for density perturbations decreased tenfold.

To tackle the limitation of the linear model, full-wave modelling with CUWA was performed for raw ELMFIRE data and the resulting CCF is presented on Fig. 8. Once again, we observe a strong decay of correlation. While the nonlinear scattering theory predicts that the four antenna configuration should be preferable [4], in our case both are at the noise level, although the four antenna configuration results in a marginally better CCF.

To confirm that this effect was caused specifically by nonlinear effects, the amplitude of density perturbations was decreased tenfold and another set of full-wave computations was performed. The resulting correlation function is shown in Fig. 9 and has the same behavior as the linear CCF in Fig. 4. Thus the nonlinear effects are capable of distorting correlation between the scattering signals and obstructing measurements.

Conclusions

Theoretical analysis of the PCR diagnostics in the linear approximation and slab geometry was performed. Analytical expression for PCR CCF was obtained. The equivalence of the three and four antenna configurations was confirmed. Theoretical results were verified with both linear and full-wave modelling. The computations have also demonstrated decorrelation of signals in the nonlinear scattering regime. Geometrical effects were also shown to play a significant role in PCR measurements for the geometry of a small tokamak like the FT-2.

Acknowledgements

This work was prepared under support of the Russian Science Foundation grant 17-12-01110. The full-wave computations were supported by the Ioffe Institute.

References

[1] Stepanov A. Yu. et al 1997 *Fusion Eng. Des.* **34-35**, 507
[2] Conway G. D. et al 1999 *Rev. Sci. Instrum.* **70** 1063
[3] Vershkov V. A. et al 2000 *Nucl. Fusion* **39** 1775
[4] Gusakov E. Z. and Popov A.Yu. 2004, *31st EPS Conf. on Plasma Phys.* ECA Vol.28G, P-1.181
[5] Gusakov E. Z and Tyntarev M. A. 1997 *Fusion Eng. Des.* **34–35,** 501
[6] Gusakov E. Z. and Kosolapova N. V. 2011 *Plasma Phys. Control. Fusion* **53,** 045012
[7] Piliya A. D. and Popov A. Yu. 2002 *Plasma Phys. Control. Fusion* **44**, 467
[8] Prisiazhniuk D. et al 2017 *Plasma Phys. Control. Fusion* **59** 025013
[9] Leerink S. et al 2012 *Phys. Rev. Lett.*, **109** 165001
[10] Niskala P. et al., 2017 *Plasma Phys. Control. Fusion* **59,** 044010
[11] Krutkin O.L. et al 2019 *Nucl. Fusion* **59** 096017
[12] Altukhov A. B. et al. 2018 *Physics of Plasmas* **25**, 082305
[13] Aleynikov P. and Marushchenko N. B., 2019 *Comp. Phys. Comm.* **241** 40